Hoggard *et al. J Cancer Metastasis Treat.* 2025;11:5
DOI: 10.20517/2394-4722.2024.105

Journal of Cancer Metastasis and Treatment

Original Article

Open Access

Check for updates

Progression of bone-metastatic prostate cancer in a mouse model treated with a novel pan-class I GLUT inhibitor (DRB18)

Nathan K. Hoggard[1], Shiyu Yuan[2,9], Marlon R. Szczepaniak[1], Megan M. Turner[3], Noriko Kantake[1], Chunmin Lo[1], Zachary D. LaRussa[1,2], Jingwen Song[2], Nigel A. Daniels[7], Jonathan A. Young[1,5], John B. Echols[8], Blake E. Hildreth III[8], Stephen C. Bergmeier[4], Xiaozhuo Chen[1,4,5], Thomas J. Rosol[1,6]

[1]Department of Biomedical Sciences, Heritage College of Osteopathic Medicine, Ohio University, Athens, OH 45701, USA.
[2]Department of Biological Sciences, College of Arts and Sciences, Ohio University, Athens, OH 45701, USA.
[3]Department of Biological Sciences, Honors Tutorial College, Ohio University, Athens, OH 45701, USA.
[4]Department of Chemistry and Biochemistry, College of Arts and Sciences, Ohio University, Athens, OH 45701, USA.
[5]Edison Biotechnology Institute, Ohio University, Athens, OH 45701, USA.
[6]Ohio Musculoskeletal and Neurological Institute, Heritage College of Osteopathic Medicine, Ohio University, Athens, OH 45701, USA.
[7]Genomics Facility, College of Arts and Sciences, Ohio University, OH 45701, USA.
[8]Department of Pathology, Heersink School of Medicine, University of Alabama at Birmingham, Birmingham, AL 35294, USA.
[9]Department of Endocrine Neoplasia and Hormonal Disorders, The University of Texas MD Anderson Cancer Center, Houston, TX 77030, USA.

Correspondence to: Dr. Thomas Rosol, Department of Biomedical Sciences, Heritage College of Osteopathic Medicine, 1 Ohio University, 349 Irvine Hall, Athens, OH 45701, USA. E-mail: rosolt@ohio.edu

How to cite this article: Hoggard NK, Yuan S, Szczepaniak MR, Turner MM, Kantake N, Lo C, LaRussa ZD, Song J, Daniels NA, Young JA, Echols JB, Hidreth BE III, Bergmeier SC, Chen X, Rosol TJ. Progression of bone-metastatic prostate cancer in a mouse model treated with a novel pan-class I GLUT inhibitor (DRB18). *J Cancer Metastasis Treat.* 2025;11:5. https://dx.doi.org/10.20517/2394-4722.2024.105

Received: 24 Sep 2024 **First Decision:** 13 Dec 2024 **Revised:** 26 Dec 2024 **Accepted:** 17 Jan 2025 **Published:** 10 Feb 2025

Academic Editor: Ciro Isidoro **Copy Editor:** Ping Zhang **Production Editor:** Ping Zhang

Abstract

Aim: Bone-metastatic prostate cancer (PCa) is a debilitating disease with few therapeutic options once androgen independence and chemotherapeutic resistance develop. Advanced PCa has metabolic vulnerabilities involving glycolysis, which is mediated by class I glucose transporters (GLUTs1-4). We previously patented DRB18, a small molecule pan-class I GLUT inhibitor that successfully inhibited the growth of a human lung cancer xenograft in mice. The purpose of this study was to determine the sensitivity of advanced PCa to GLUT antagonism using DRB18.

Methods: Bioinformatics was performed on human and canine PCa datasets to determine the clinical expression of class I GLUTs. Glucose uptake and cell viability in response to DRB18 were measured *in vitro*. Tibias of athymic mice were inoculated with Ace-1 canine PCa cells and treated with DRB18. The combination of DRB18 with cytotoxic docetaxel was assessed *in vitro*.

Results: Expression of important class I GLUTs and glycolysis genes increased during PCa progression in men and dogs. DRB18 reduced cancer cell glucose uptake and cell viability in a dose-dependent manner. Half-maximal inhibitory concentrations (IC_{50}) ranged from 20-30 μM. DRB18 did not prevent intratibial PCa growth *in vivo* and had toxic effects at higher concentrations. DRB18 and docetaxel combination therapy and gene expression data from publicly available human PCa samples indicated docetaxel treatment does not stimulate glucose-related metabolic pathways.

Conclusion: GLUT1 inhibition alone or with combination therapy may not be appropriate for bone-metastasis inhibition. The results contribute to evidence that suggests bone metastatic PCa is not glucose dependent.

Keywords: Prostate cancer, bone metastasis, glycolysis, glucose transporter, DRB18, Ace-1, dog, preclinical model

INTRODUCTION

Prostate cancer (PCa) is a common malignancy that affects men worldwide[1,2]. PCa is generally a slowly progressive disease, but some men develop advanced disease, which is usually complicated by bone metastasis[3]. Effective therapies for advanced PCa, including bone metastasis, are limited and short-lived[4]. The androgen receptor (AR) signaling pathway is an early driver of PCa and an important therapeutic target[5]. PCa eventually develops resistance to drugs targeting the androgen-AR pathway (androgen-independent stage) and the U.S. Food and Drug AdministraBon (FDA)-approved cytotoxic chemotherapeutic docetaxel for bone-metastatic disease[6,7]. New therapies that can mitigate advanced, androgen-independent PCa are needed.

A century ago, Otto Warburg described the tendency of malignant tumor cells to increase glucose consumption and catabolism (glycolysis) to generate adenosine triphosphate (ATP) and lactate, even in the presence of adequate oxygen (aerobic glycolysis)[8,9]. Thus, tumor cells can depend on glycolysis alone, avoiding prototypical cellular metabolic pathways of the tricarboxylic acid cycle (TCA) and oxidative phosphorylation. If large amounts of glucose can be transported into a cell and catabolized through glycolysis, sufficient ATP to maintain cellular homeostasis and support growth can be generated[10].

Cellular uptake of glucose is primarily mediated by transmembrane channel glucose transporters (GLUTs)[11]. The facilitative GLUT family includes 14 transporter proteins divided into classes based on structure and function[12]. Class I GLUTs (GLUTs 1-4) are the most extensively studied. The class I GLUTs known to be important in cancer, GLUT1 and 3, have cellular and systemic regulatory mechanisms in normal physiology[13,14]. GLUT1 is variably expressed in most normal tissues and cancers, while GLUT3 is a high-affinity glucose transporter expressed in rapidly proliferating and glucose-dependent tissues (e.g. neurons)[11,12]. Regulatory factors of cellular GLUTs and translocation to the plasma membrane vary depending on inherent cell functions and the microenvironment. For example, GLUT4 is primarily regulated by insulin[15]. In cancer, however, GLUT1 and 3 are primarily upregulated by the oncoprotein cellular myelocystomatosis (c-MYC) and tissue hypoxia, which is mediated by hypoxia-inducible factor-1 (HIF-1) alpha and beta subunits[16].

Metabolic heterogeneity exists between and within tumor types[17]. Contrary to the "Warburg effect", low-grade PCa confined to the prostate gland is metabolically tuned toward oxidative phosphorylation, which may include lipids as a fuel source, reflecting the slow growth during this stage[18,19]. However, basic, preclinical, and clinical studies suggest higher grade and advanced PCa rely on accelerated glucose uptake[20,21]. Factors within the microenvironment, including metabolic rate, oxygen tension, and pH, can influence tumor metabolism and growth[22,23]. Bone, an important site of PCa metastasis, is a relatively hypoxic environment. The cortical and trabecular endosteum of the metaphysis, where metastatic PCa is often located, have oxygen pressures as low as 13 mm Hg (normal is 25-40 mm Hg)[24]. This low oxygen pressure is thought to limit oxidative phosphorylation in favor of anaerobic processes, such as glycolysis[25]. This suggests that inherent cancer cell metabolism and the bone microenvironment direct metastatic PCa toward glycolysis.

Reviews on the therapeutic targeting of glycolysis or GLUTs in cancer have been published[26,27]. Early investigations into GLUT inhibition raised concerns, since the inhibitors targeted only a single GLUT or had low specificity, requiring a higher dose that could adversely impact non-cancerous tissues[26] The introduction of newer GLUT inhibitors with pan-transporter inhibition has helped address these concerns. DRB18 is a synthetic small molecule patented at our institution that selectively and specifically inhibits class I GLUTs (GLUTs 1-4), with a half-maximal inhibitory concentration (IC_{50}) of less than 10 μM in multiple cancer cell lines[28,29]. Advantages of DRB18 over earlier GLUT antagonists are: (1) inhibition of multiple GLUTs (pan-GLUT inhibition) and (2) increased chemical stability in serum due to amide bonds[29,30]. DRB18 successfully inhibited the subcutaneous growth of the human lung cancer cell line A549 xenograft in *NU/J* nude mice[29]. The potency of DRB18 in metabolism research has been reported[31,32] . Only one study reported the anti-tumor efficacy of a small molecule GLUT1 antagonist (STF-31) in a mouse model of PCa[33]. However, no proof-of-concept preclinical or clinical studies targeting GLUTs in bone metastatic, androgen-independent PCa have been performed.

The purpose of this study was to determine the sensitivity of advanced PCa to GLUT antagonism using DRB18 as a model compound. The *in vivo* efficacy and safety of GLUT antagonism were tested in a mouse model of bone metastatic PCa.

METHODS

Cell lines and cell culture

Canine PCa cell lines Ace-1, Probasco, Leo, and LuMa were previously generated by our lab and are useful to study mouse models of androgen-independent PCa with bone metastasis[34-38]. Primary cell cultures for each cell line were derived from spontaneous PCa of neutered male dogs. Ace-1 cells were transduced with a retroviral vector containing a yellow fluorescent protein (YFP) and luciferase (LUC) dual reporter gene (Ace-$1^{YFP\text{-}LUC}$)[34]. The human PCa cell line, PC3, was kindly provided by Dr. Evan Keller (University of Michigan). The Madin-Darby canine kidney (MDCK) epithelial cell line was purchased from American Type Culture Collection (ATCC). Ace-1 and PC3 have undetectable AR gene expression and protein[34,39]. PCa and MDCK cells were cultured in Dulbecco's Modified Eagle Medium (DMEM)/F12 - GlutaMax™ (17.5 mM glucose; Gibco, Thermo Fisher Scientific, Waltham, MA) containing 10% fetal bovine serum (FBS) (Gibco, Thermo Fisher Scientific), 1% penicillin/streptomycin (Life Technologies), and 100 μg/mL Normocin (InvivoGen, San Diego, California). Ace-1 cells were also grown in DMEM low glucose (4.5 mM glucose; Gibco) and RPMI 1,640 media (11.1 mM glucose; Gibco, Thermo Fisher Scientific) with the above supplements (see Supplementary Materials). All cells were serially passaged using TrypLE™ (Gibco, Thermo Fisher Scientific) and maintained at 37 ºC with 5% CO_2 in a humidified atmosphere. The passage numbers for the established canine cell lines were below 30.

Transcriptome analysis of human and canine prostate cancer

Human primary and metastatic PCa expression data were downloaded from Gene Expression Omnibus (GEO) accessions GSE80609[40] and GSE77930[41], respectively. Canine expression data were downloaded from GSE122916[42]. RNA-seq raw gene counts (GSE80609 and GSE122916) were uploaded to R Studio (Version 2024.04.2 + 764) and processed in Bioconductor using edgeR (Version 4.2.1)[43]. Trimmed Mean of M-values (TMM) normalization size factors were calculated to adjust for samples with differences in library size. Microarray data (GSE77930) as batch-normalized log2 intensities were processed and normalized in R/Bioconductor, followed by expression analysis using limma (Version 3.60.2)[44]. If two probes mapped to the same gene, the probe with the greatest positive or negative log2 fold change was used for analysis.

RNA-sequencing was performed on the four canine PCa cell lines. RNA was isolated using PureLinkTM RNA mini kit (Invitrogen). The RNA concentration and integrity were measured using a 2100 Bioanalyzer (Agilent, Santa Clara, CA, USA) at the Ohio University Genomics Facility. Samples with RNA integrity numbers higher than 9 were used for RNA sequencing. Library preparation, next-generation sequencing, and primary differentially expressed gene (DEG) analysis were performed (McDonnell Genome Institute, Washington University, St. Louis, MO). Briefly, samples were sequenced on an Illumina NovaSeq 6000 platform (Illumina Inc., San Diego, CA, USA). Basecalls and demultiplexing were performed with Illumina's bcl2fastq software. For canine samples, RNA-seq reads were aligned to the dog reference genome assembly canFam6 (Dog10K_Boxer_Tasha; https://www.ncbi.nlm.nih.gov/datasets/genome/). Gene counts were derived from the number of uniquely aligned unambiguous reads by Subread:featureCount (Version 2.0.3).

Sequencing data of canine non-cancerous prostate retrieved from the GEO accession GSE122916 were used as a comparison control for each of the four canine PCa cell lines to calculate DEGs. Briefly, datasets were trimmed using fastp (Version 0.23.2). The trimmed collections were aligned to genome assembly canFam6 GCF_000002285.5/) using HISAT2 (Version 2.2.1) with default settings, and alignment was generated using MultiQC (Version 1.11). Gene counts corresponding to the canFam6 annotation were generated from the alignment files using featureCounts (Version 2.0.3) to produce count tables. Gene counts were processed in the R/Bioconductor and edgeR as above. The TMM size factors and the count matrix were then imported into limma for weighted likelihood calculation based on the gene-sample mean-variance relationship, and limma's voomWithQualityWeights (Version 3.50.1) was used to transform the count matrix into moderated log2 counts-per-million. Differential expression analysis was then conducted between samples using the Benjamini-Hochberg adjustment method.

Gene expression profiles were visualized as heatmaps by utilizing Morpheus heatmapping software from the Broad Institute (https://software.broadinstitute.org/morpheus).

Quantitative real-time polymerase chain reaction

RNA was extracted from PCa and MDCK cells using a Qiagen RNeasy Mini Kit (Qiagen, Hilden, Germany). Total RNA was reverse transcribed into cDNA using the Superscript IV First Strand cDNA synthesis kit (Invitrogen) to 1.25 µg/µl. Quantitative real-time polymerase chain reaction (qRT-PCR) was performed for the reference housekeeping gene *GAPDH* and GLUTs 1-4 (*SLC2A1*, *SLC2A2*, *SLC2A3*, *SLC2A4*). MDCK cells, immortalized epithelium isolated from adult dog kidneys, served as normal (non-cancerous) control cells for comparison. Canine primer pairs were designed using the NCBI Primer-BLAST software[45]. Canine and human primer pairs are listed in Table 1. A gene with a Ct value of 35 or greater was considered not expressed. The thermal cycle conditions were: 95 °C, 3 min; (95 °C, 10 s; 55 °C, 30 s; 75 °C, 30 s) × 39; 95 °C, 1 min; 55 °C, 1 min. Target gene expression was normalized by the reference gene (*GAPDH*) and quantified using the $2^{-\Delta\Delta Ct}$ method to calculate the fold change relative to MDCK cells.

Table 1. Primers used for qRT-PCR

Gene	Species	Forward (5′-3′)	Reverse (5′-3′)
GAPDH	Canine	AGCCAAATTCATTGTCATACCAGG	CCCACTCTTCCACCTTCGAC
SLC2A1		CCTGCAGTTTGGCTACAACAC	AGGACTTGGCCAGTTTCGAG
SLC2A2		TGTGTGTGCCATCTTCATGTCC	AGAACTCTGCCACCATGAACCA
SLC2A3		CTTCAGATCGCGCAGCTACC	TGCATCTTTGAAGATTCCTGTTGAG
SLC2A4		GCTTCTGCAACTGGACAAGCAA	AAGTCAGCCGAGATCTGGTCAA
GAPDH	Human	GCAAATTCCATGGCACCGTC	AGCATCGCCCCACTTGATTT
SLC2A1		TCTGGCATCAACGCTGTCTTC	CGATACCGGAGCCAATGGT
SLC2A3		CGTTGTTGGAATTCTGGTGGC	CTTAGCATTCTCCTCTTCTTTT
SLC2A4		GCCATGAGCTACGTCTCCATT	GGCCACGATGAACCAAGGAA

qRT-PCR: Quantitative real-time polymerase chain reaction.

Protein extraction and immunoblotting

PCa cell lines were cultured to approximately 60%-80% confluence in 6-well plates as singlets, without technical replicates, prior to protein extraction. Cells were lysed using RIPA lysis buffer (Thermo Fisher Scientific, Waltham, MA). Total protein (10 μg) was separated by sodium dodecyl sulfate polyacrylamide gel electrophoresis (SDS-PAGE) and transferred to a polyvinylidene fluoride (PVDF) membrane. Membranes were blocked with 5% non-fat milk and probed with primary antibodies to GLUT1 (1:1000; Proteintech 21829-1-AP) and β-actin (1:1000; Abcam ab8227). Membranes were incubated with horseradish peroxidase (HRP)-conjugated secondary antibodies (1:2000; Cell Signaling Technology 7074) and imaged by chemiluminescence using a BioRad ChemiDoc MP Imaging System.

Chemical inhibitors, DRB18 and docetaxel

DRB18 and docetaxel (DTX) were purchased as a powder (Selleck Chemicals, Houston, TX). Additional DRB18 for some experiments was synthesized as previously reported[46]. Solutions were prepared by dissolving the compound in 100% dimethyl sulfoxide (DMSO). Serial dilutions were performed using complete cell culture media.

DRB18 cell viability and dose-response curves

Cell viability assays were performed using resazurin (Cell Signaling Technology, Danvers, MA) according to the manufacturer's protocol. PCa cell lines and MDCK cells were seeded into black-walled, clear bottom 96-well plates (Thermo Fisher Scientific, Waltham, MA) in triplicate at a density of 10,000 cells/well. 24 h later, cells were treated with 5-50 μM DRB18 for 24 h. Vehicle-treated (0.5% DMSO) cells were used as controls for each replicate. Fluorescence was measured at excitation 550 nm and emission 590 nm using a microplate reader (SpectraMax iD5, Molecular Devices, LLC., San Jose, CA). Relative cell viability was calculated by normalizing to wells containing media only (blanks) and displayed as a percentage (0%-100%) of DMSO-only treated cells. One hundred percent was defined by fluorescence intensity of control (DMSO-only treated) cells after subtraction of background fluorescence (blanks).

Glucose uptake assay

The inhibitory activity of DRB18 on glucose transport in Ace-1 cells was determined by measuring the uptake of 2-deoxy-d-[^{3}H] glucose. Cells were seeded into 24-well plates in triplicate, washed with serum-free DMEM two times, and incubated for 2 h to minimize the influence of serum. Cells were washed with Krebs Ringer Phosphate (KRP) buffer three times and incubated for 30 min for preparation for glucose uptake. Cells were incubated for 15 min at 37 °C with 5, 10, 20, or 50 μM DRB18. Vehicle-treated (0.7% DMSO) cells were used as controls. A mixture composed of 5 mM glucose and 1% 2-deoxy-D-[^{3}H] glucose was added to initiate glucose uptake. After thirty minutes, the cells were washed with cold phosphate-buffered

saline (PBS) three times to stop glucose uptake. During this process, radioactive glucose remaining outside of cells was removed. NaOH (0.2 M) was then added to lyse the cells. Radioactive glucose inside the cells was transferred into scintillation vials for counting (LS 6500 Scintillation Counter, Beckman Coulter).

Intratibial tumor inoculation and compound injections

Nude mice at 8 weeks of age (n = 16) were maintained under isoflurane anesthesia (2.5%) and oxygen mixture in dorsal recumbency during intratibial (IT) injection. Ace-1$^{YFP\text{-}LUC}$ cells (50,000 cells suspended in 10 µL of sterilized Dulbecco's phosphate-buffered saline (DPBS; Gibco, Thermo Fisher Scientific) were loaded in a Hamilton syringe with a 27-gauge needle. The needle was placed through the patellar tendon/ligament and proximal tibia metaphysis. Two mice in the treatment group received IT injections in both the left and right tibias due to an initial false-negative bioluminescent signal. The limb having the highest bioluminescent signal (photons/sec/cm^2) at each time point was selected for analysis. DRB18 treatment began on the day of tumor inoculation. Mice were allocated into control and treatment groups based on the bioluminescent signal on the day of injection to equalize initial signals in the groups. Control mice (n = 8) were treated with PBS/DMSO (1:1, v/v), and treatment mice (n = 8) were administered DRB18 in PBS/DMSO solution (1:1, v/v). Mice were initially given intraperitoneal injections with vehicle or DRB18 (20 mg/kg) every 48 h. After 5 d, the frequency of injection was reduced to every 72 h. Following an additional 11 d, the dose was reduced to 10 mg/kg every 72 h. The starting DRB18 dose was selected based on the *in vitro* IC_{50} values of Ace-1 as determined by cell viability assay. To derive an *in vivo* dose from *in vitro* IC_{50} values, two assumptions were made: 1) the density of a mouse is approximately 1 g/mL, and 2) the compound is evenly distributed throughout the body.

Bioluminescent imaging

IT tumor growth was evaluated by bioluminescent imaging weekly for 3 weeks, starting on the day of tumor inoculation. D-Luciferin (15 mg/mL; Perkin Elmer, Waltham, MA) dissolved in DPBS was injected intraperitoneally in each mouse (150 mg/kg) prior to general anesthesia and imaging using a 1 mL insulin syringe. The IVIS 100 (Caliper Life Sciences, Hopkinton, MA) was used. The photon flux (total photons/sec) was measured for each region of interest using Living Image software version 2.50 (Caliper Life Sciences).

Plasma biochemical and metabolic parameters

Five days following the final DRB18 injection, mice were fasted for 4 h and euthanized by combined CO_2 asphyxiation and cervical dislocation in accordance with the AVMA Guidelines for the Euthanasia of Animals. Blood was collected immediately postmortem from each mouse by cardiac puncture. Blood glucose was determined using a Henry Schein® True Metrix® Pro glucometer and test strips. The remaining blood was placed in blood collection tubes containing lithium heparin (BD Microtainer®, Becton, Dickinson and Company, Franklin Lakes, NJ) and centrifuged at 2500 RPM for 15 min to separate the plasma. Approximately 100 µL of plasma was collected from each mouse, placed in 0.5 mL Eppendorf tubes, and stored at -80 ºC. Plasma was thawed for measurement of insulin and triglycerides using commercial mouse enzyme-linked immunosorbent assay (ELISA) kits. The mouse insulin ELISA kit (ALPCO, Salem, NH) was used. Absorbance was measured with a microplate reader (FLUOstar OPTIMA, BMG Labtech, Cary, NC), and the final concentrations were calculated based on the standard curve. Plasma triglyceride and cholesterol concentrations were determined using Infinity triglyceride and cholesterol kits (Thermo Fisher Scientific, Middletown, VA). Absorbance was measured with a microplate reader (Synergy HT, BioTek Instruments, Richmond, VA), and the final concentrations were calculated based on the standard curve.

Preclinical and autopsy findings

Mice were weighed and evaluated daily, including changes in activity, mentation, or ambulation. A gross examination was performed on each mouse following death or euthanasia. The heart, liver, and kidneys were weighed. Mean relative organ weights were determined by dividing the organ weight by the final antemortem body weight.

Histopathology

Thoracic and abdominal organs were removed and, along with the pelvic limbs, fixed in 10% neutral-buffered formalin for 48-72 h. Pelvic limbs were decalcified in 10% ethylenediaminetetraaceBc acid (EDTA, pH 7.6) for 48-96 h. Tissues were rehydrated by soaking in 1X PBS prior to processing. Tissues were paraffin-embedded, sectioned at 4-5 µm, mounted on glass slides, stained with hematoxylin and eosin (H&E), and cover slipped. The pelvic limbs (femur and tibia) and gastrointestinal tract (pancreas, jejunum, ileum, cecum, and colon) were evaluated by light microscopy.

In vitro docetaxel treatment

To determine the sensitivity to DTX *in vitro*, Ace-1 cells were seeded onto 96-well plates, and cell viability was measured using resazurin dye as above. Ace-1 cells were treated with 0-1000 nM DTX for 24 h or 72 h. DMSO-treated (0.01%) cells served as controls.

To determine the effects of DTX on gene expression *in vitro*, Ace-1 cells were seeded on a 24-well plate at a density of 10,000 cells/well in triplicate and treated with 0 nM, 5 nM, or 10 nM DTX for 72 h. RNA isolation, cDNA synthesis, and quantification were performed as above.

Cell viability after combination treatment

The effects of combined DRB18 (10 µM) and DTX (10-1000 nM) on cell viability were determined using Ace-1 and PC3 cells. Cells were treated with combinations of compounds for 24 h prior to the addition of resazurin and fluorescence measurement as described above. Cells in each well received the same concentration of DMSO (0.11%).

Transcriptome analysis of human prostate cancer treated with docetaxel

To determine if DTX treatment significantly altered pathways related to cancer cell metabolism in metastatic human PCa, expression data were downloaded from Gene Expression Omnibus accession GSE74685[47] as described above. Genes were filtered to keep only genes with an interquartile range > 0.5 prior to DEG analysis. Gene set enrichment analysis (GSEA) was performed on the gene expression results using fgsea with the H, C2, C3, and C5 collections of gene sets from MSigDB.

Statistical analysis and graphics

All data were displayed as mean ± standard deviation unless otherwise noted. Statistical analyses with two comparison groups used an unpaired Student's *t*-test. A one-way analysis of variance (one-way ANOVA) with Dunnett's posthoc test was used for comparisons between more than two groups. Dose-response curves were generated using a four-parameter (four-parameter logistic) nonlinear regression analysis (log of concentration vs response - variable slope). The bottom plateau for PC3 and Probasco cell dose-response curves was constrained by Y = 0. Outliers from biological samples were identified using Grubbs's test (alpha value ≤ 0.01). Identified outliers (n = 1 for plasma insulin) were removed for statistical comparisons. Data with $P < 0.05$ were considered statistically significant. Statistics, calculations, and graphical display were performed using GraphPad Prism (Version 6.03, La Jolla, CA).

RESULTS

Class I GLUTs and glycolysis in human and canine PCa

Gene expression of class I GLUTs, regulators of GLUTs, and proteins involved in the glycolytic pathway were investigated in human and canine PCa using publicly available datasets and canine PCa cell lines [Figure 1A-C]. Human and canine tumors had similar gene expression patterns relative to non-cancerous controls. However, canine PCa had greater gene expression for glycolysis than human PCa, including locally advanced primary tumors. Importantly, the relative gene expression of the canine cell lines recapitulated that of canine primary PCa [Figure 1B].

Human and canine PCa expressed genes for multiple class I GLUTs, revealing the importance of pan-GLUT inhibition. Genes for GLUTs 1, 3, and 4 were expressed by PCa and non-cancerous prostate, while GLUT2 was not expressed by either tissue. GLUTs 1 and 3 gene expression was upregulated in human primary PCa relative to the non-cancerous gland, and expression of these GLUTs also increased in bone metastases compared to primary cancers, though only GLUT3 reached significance ($P < 0.0001$; Figure 1A and C). GLUT3 was the predominant class I GLUT in both human and canine PCa. Interestingly, gene markers of hypoxia (*HIF1A* and *CA9*) known to regulate GLUTs 1 and 3 were not upregulated in primary or bone metastatic PCa or PCa cell lines, suggesting *MYC* or other pathways independent of tissue hypoxia may be involved in GLUT1 and 3 regulation. These data suggested human and canine PCa upregulate GLUTs 1 and/or 3 in the progression from localized tumors to bone metastasis.

qRT-PCR of GLUTs 1 and 3 in human and canine PCa cell lines was consistent with the clinical and RNA-seq data [Figure 1D and E]. Absolute gene expression, indicated by cycle threshold (Ct) value, indicated GLUT3 was often the favored class I GLUT [Supplementary Table 1]. Ace-1 cells, however, only expressed the gene for GLUT1. Gene expression for canine GLUTs 2 and 4 using previously validated and published primer pairs was not detected in any canine PCa cell line[48]. The trend in GLUT1 protein determined by immunoblotting for each cell line was consistent with relative qRT-PCR gene expression [Figure 1F].

DRB18 inhibited the growth of PCa cells and reduced glucose uptake *in vitro*

DRB18 reduced the cell viability of PCa cell lines in a dose-dependent manner, leading to an equivalent relative IC_{50} of 22-38 μM following exposure to DRB18 for 24 h [Figure 2A]. The relative IC_{50} was calculated from the midpoint between the top and bottom plateaus of the dose-response curve. Ace-1, Leo, and PC3 cells had similar sigmoidal dose-response curves that nearly reached 0% cell viability relative to control cells at high DRB18 concentrations. Most PCa cell lines were resistant to DRB18 at concentrations less than 20 μM and had an abrupt increase (steep slope) in sensitivity to DRB18 between 20 and 30 μM. LuMa was resistant to higher doses of DRB18. Increasing the DRB18 exposure time to 72 h decreased the relative IC_{50} of Ace-1 by approximately 10 μM [Supplementary Figure 1A]. The type of media, but not the glucose concentration, affected cell viability in response to DRB18 [Supplementary Figure 1B and C]. PCa cell lines had a lower sensitivity to DRB18 compared to previously tested cancer cell lines[29].

DRB18 rapidly inhibited glucose uptake in Ace-1 cells [Figure 2B], demonstrating potent specificity for class I GLUTs, as expected. Cells were treated with 0, 10, 20, and 50 μM of DRB18 for 15 minutes, and the uptake of radioactive glucose was measured. Ace-1 cells had an IC_{50} in radioactive glucose uptake at DRB18 concentrations of 20 μM. DRB18 had a similar effect on the Probasco cell line [Supplementary Figure 1D].

DRB18 selectively inhibited PCa cells *in vitro*

The efficacy of DRB18 was tested on MDCK cells. The inhibitory effect of DRB18 on cell viability was greater in Ace-1 compared to MDCK cells, particularly at 30 μM or higher [Figure 2C].

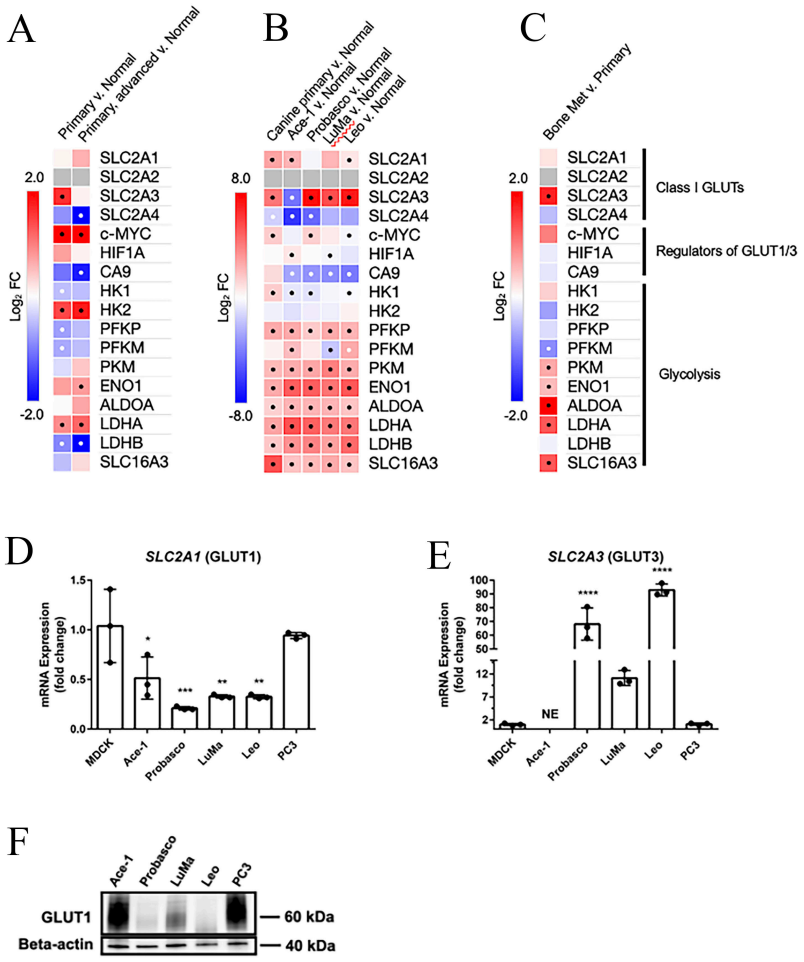

Figure 1. Expression of class I GLUTs and associated pathways in human and canine PCa and cell lines. (A-C) Gene expression heatmaps were generated from publicly available human or canine clinical samples and canine PCa cell lines. "Normal" indicates non-cancerous prostate gland for the respective species, human or canine. Scale bars indicate the $\log_2$ fold change (Log_2 FC) in gene expression between groups, as displayed above the heatmaps. Black or white dots indicate the significance of $P < 0.05$ or smaller reached between groups; Gray boxes indicate the gene was not detected. (D) and (E) Gene expression of GLUTs 1 and 3 was confirmed by qRT-PCR of human and canine PCa cell lines *in vitro*. Cells were seeded in triplicate and normalized to the housekeeping gene, *GAPDH*. The relative expression of each cell line was calculated and statistically analyzed by one-way ANOVA relative to control (MDCK) cells. Data were displayed as mean ± SD. *$P < 0.05$; **$P < 0.01$; *** $P < 0.001$; ****$P < 0.0001$. NE: not expressed. (F). GLUT1 was produced by PCa cell lines *in vitro*. GLUTs: Glucose transporters; PCa: Prostate cancer; MDCK: Madin-Darby canine kidney cells.

The maximum tolerable concentration of DRB18 did not reduce PCa growth in bone

The tibias of all 16 mice inoculated with Ace-1$^{\text{YFP-LUC}}$ cells developed tumors detectable by bioluminescence imaging. Representative images for control and treated groups at each time point are shown in Figure 3A. The bioluminescent signal of intratibial tumors in control and treated mice was not significantly different during the 3-week study [Figure 3B]. The *in vivo* dose of DRB18 was maximized based on evidence of systemic toxicity. The *in vivo* dose of DRB18 of 20 mg/kg every 48 h led to a statistically significant loss of body weight beginning the first week of treatment [Figure 3C].

To determine if DRB18 administration in nude mice affected glucose homeostasis and its association with weight loss, blood was collected from control ($n = 8$) and treated ($n = 4$) mice five days following the final DRB18 injection. Blood glucose, plasma insulin, and plasma triglycerides were measured [Figures 3D-G]. Blood glucose and plasma insulin concentrations were not statistically different between groups, though

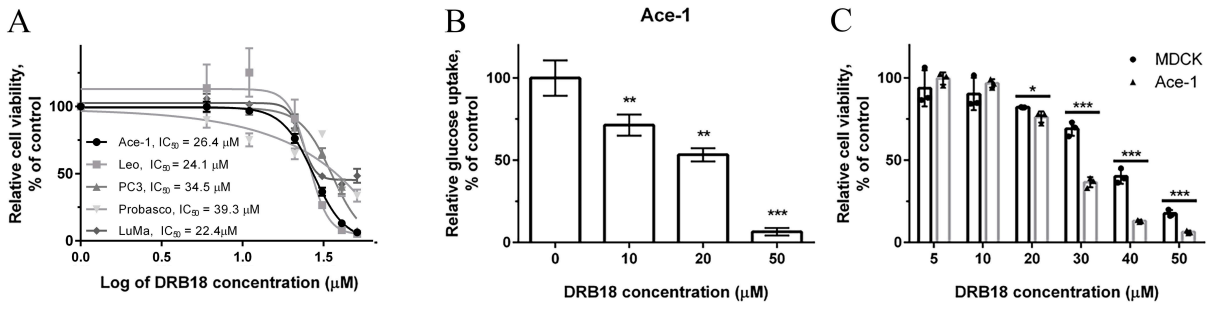

Figure 2. *In vitro* dose-dependent effects of DRB18 on PCa cell lines and non-cancerous cells. (A) Five PCa cell lines were treated with 5, 10, 20, 30, 40, and 50 μM DRB18 for 24 h. DRB18 reduced relative cell viability in a dose-dependent manner; (B) DRB18 inhibited glucose uptake in a dose-dependent manner. Ace-1 cells were seeded in triplicate and treated with increasing doses of DRB18 for 15 min. Uptake of 2-deoxy-D-[3H] glucose was quantified by scintillation. One-way ANOVA; (C) Cell viability of Ace-1 cells and the canine kidney epithelial cell line MDCK following treatment with 5, 10, 20, 30, 40, and 50 μM DRB18 for 24 h. Cells were seeded in triplicate. Data were displayed as mean ± SD. Unpaired *t*-tests. *$P < 0.05$; **$P < 0.01$; *** $P < 0.001$. PCa: Prostate cancer; MDCK: Madin-Darby canine kidney cells.

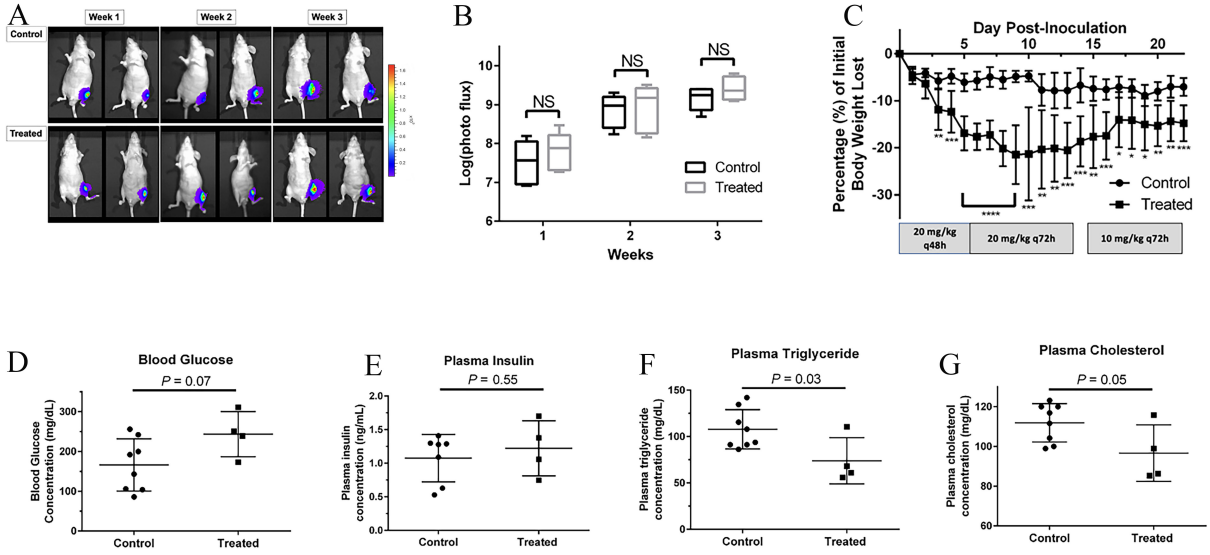

Figure 3. *In vivo* efficacy and safety of DRB18. Ace-1$^{YFP\text{-}LUC}$ cells were injected into the proximal tibias of male, 8-week-old nude mice (n = 16) initially treated with 20 mg/kg DRB18 or DMSO/PBS (1:1; v:v) for three weeks by intraperitoneal injection every 48 h. Surviving mice (n = 12) were sacrificed after 3 weeks. (A) Representative bioluminescent images of control (top row) and treated (bottom row) mice. Images were taken once weekly for 3 weeks. Bioluminescent intensity is proportional to the number of viable tumor cells and reflects tumor size. The photon flux (photons/second/region of interest) scale bar applies only to the left adjacent images; (B) Quantification of bioluminescent intensity for control and treated mice for each week of the study. DRB18 did not reduce the growth of intratibial tumors compared to controls. Box plot. NS: Not significant. Unpaired *t*-test at each time point; (C) Change in body weight between control and treated mice from study start to termination. The DRB18 concentration administered and frequency are listed below. q: *quaque*.Unpaired *t*-tests; (D-G) Changes in treatment-related metabolic biochemical parameters at the study's termination between control (n = 8) and treated (n = 4) mice. Unpaired *t*-tests. *$P <$ 0.05; **$P < 0.01$; ***$P < 0.001$; ****$P < 0.0001$.

both trended upward in treated mice. Plasma triglyceride concentration was lower in the treated mice ($P = 0.03$). Plasma cholesterol trended downward in treated mice but did not each statistical significance ($P = 0.05$).

Four out of eight (50%) treated mice died during the study. All mice (n = 16) received complete autopsies and histopathologic examination to evaluate intratibial tumor growth and causes of weight loss. Inoculated

tumors filled the metaphyseal region of tibias and extended through cortical bone, resulting in a robust periosteal reaction. Microscopic morphology of the tumors and affected bone were similar between groups [Figure 4A and B]. Treated mice had mild peritonitis associated with DRB18 administration. Peritonitis was not observed in control mice. In addition, treated mice had peritoneal fibrosis and fat necrosis [Figure 4C and D]. Three treated mice had focal fat necrosis in the mesentery or body wall corresponding to DRB18 injection sites. The relative weights for the heart, liver, and kidneys were not statistically significant between groups [Supplementary Table 2].

Docetaxel did not potentiate DRB18 *in vitro*

Since DRB18 did not reduce intratibial tumor growth as a single compound agent, combination therapy with docetaxel was investigated *in vitro*. DTX is an FDA-approved cytotoxic chemotherapeutic administered to men with refractory and metastatic androgen-independent PCa.

DTX reduced Ace-1 cell viability in a dose- and time-dependent manner [Figure 5A]. Next, Ace-1 cells were treated with increasing concentrations of DTX for 72 h. Treatment with DTX increased gene expression for GLUTs 1 and 3 in a dose-dependent manner [Figure 5B and C]. While DTX increased PCa GLUT expression *in vitro*, DRB18 and DTX together did not potentiate their anti-cancer activity. A fixed concentration of DRB18 (10 μM) in combination with DTX produced no or relatively small reductions in cell viability compared to either compound administered alone to Ace-1 and PC3 cells over 24 h [Figure 5D and E].

Transcriptome alterations in human PCa treated with docetaxel

Using clinical and expression data[41,47], we separated metastatic PCa samples into two groups: metastases treated with first-line therapy (androgen and androgen pathway inhibitors) and metastases treated with first-line therapy plus DTX. Gene expression from all metastases treated with and without DTX were compared. In addition, bone metastases treated with and without DTX were investigated. No gene sets pertaining to glucose uptake or glycolysis reached statistical significance between metastatic groups treated with or without DTX [Figure 5F]. Differentially expressed genes (DEGs) were also investigated in response to metastases treated with and without DTX. Five and two genes were significantly differentially expressed between combined metastases and bone-only metastases, respectively, treated with and without DTX. Of the seven DEGs, only one was associated with cell metabolism. The gene encoding phosphotyrosine interaction domain containing 1 (*PID1*) was significantly ($P = 0.04$) downregulated in bone metastases treated with DTX.

DISCUSSION

Glycolysis is a targetable metabolic vulnerability of cancer[8]. The influx of glucose to nourish cancer cells is mediated by GLUTs. The current study determined the validity of targeting class I GLUTs in a preclinical mouse model of bone metastatic PCa using the pan-class I GLUT inhibitor, DRB18. We found that some GLUTs were upregulated in primary and bone metastatic human and primary canine PCa. GLUT antagonism via DRB18 also inhibited PCa cells *in vitro*. However, DRB18 did not reduce PCa growth following inoculation of tumor cells in the tibias of nude mice.

GLUT antagonists alone may not be therapeutically effective for all types of cancer and their clinical stages. In addition, cancer heterogeneity and the microenvironment will influence metabolism. The success of prior preclinical studies using DRB18 or other GLUT antagonists as single anti-cancer agents may have depended on the reliance of the specific cancer types on glucose transport[29,49]. While we and others have shown increased class I GLUT and glycolysis-related genes in PCa compared with normal prostate,

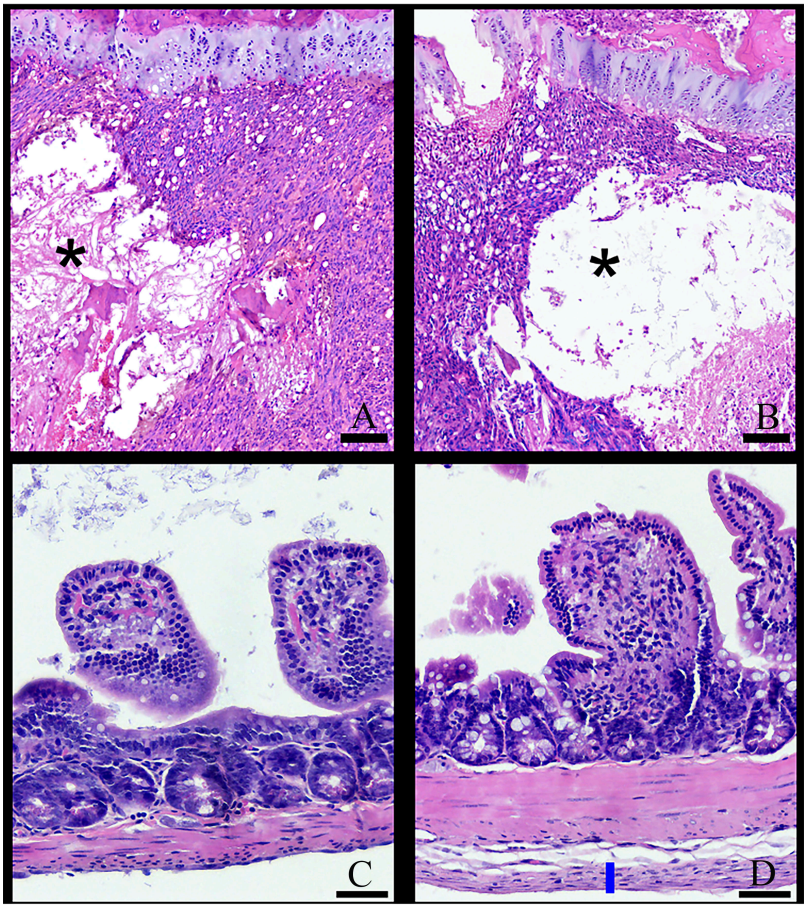

Figure 4. Histopathology of intratibial tumors and abdominal pathological changes in control (*n* = 8) and treated (*n* = 4) male, 11-week-old nude mice. Intratibial tumors that grew in the metaphyses of control (A) and treated (B) mice were microscopically similar (H&E stain; original magnification 10x). Central areas contained tumor cell necrosis and fragments of necrotic, lamellar trabecular bone (*). Scale bar: 100 µm; (C) Ileum from a control mouse (H&E stain; original magnification: 20x); (D) Ileum from a DRB18-treated mouse at day 21 with serosal fibrosis (blue vertical bar; H&E stain; original magnification: 20x). Scale bar: 50 µm.

localized and metastatic PCa may be less glycolytically dependent compared to other malignancies[50,51]. A comparison of metabolism endpoints between cancer types is needed to further investigate intertumoral metabolic heterogeneity.

The tissue microenvironment also influences PCa cell-based metabolism. The PCa cell line PC3 had different metabolic dependencies between intraosseous and subcutaneous growth in mice[52]. The subcutaneous microenvironment directed PC3 cells toward glycolysis, while the bone marrow promoted oxygen-dependent metabolism. Recent studies using clinical gene expression data are supportive, finding genes and gene sets for oxidative phosphorylation were significantly upregulated in bone metastatic samples compared to primary PCa[53,54]. The bioinformatic and clinical FDG data analyzed indicated a role for glucose transport and glycolysis in PCa progression and bone metastasis. This may be due to glucose used in support of oxidative phosphorylation, or alternatively, glycolysis may be a secondary or tertiary metabolic pathway in bone metastatic PCa. Recent data from rodent preclinical and clinical bone metastatic PCa studies suggest that PCa utilizes oxidative phosphorylation, possibly explaining the lack of effectiveness of DRB18 in this study.

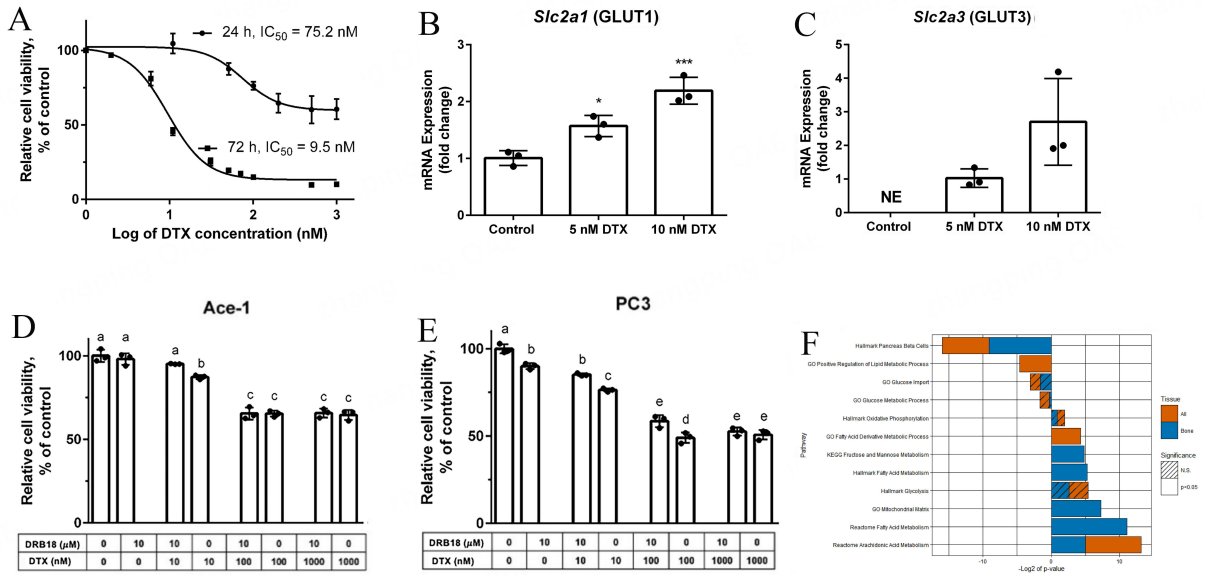

Figure 5. Effect of docetaxel (DTX) on PCa metabolism *in vitro* and *in silico*. (A) Dose-response curves following treatment of Ace-1 cells with increasing concentration of DTX for 24 h (top curve) and 72 h (bottom curve); (B and C) Ace-1 cells were treated with increasing concentrations of DTX for 72 h, resulting in increased gene expression of GLUTs 1 and 3 in a dose-dependent manner. One-way ANOVA. Statistical comparisons are between both treated groups and control (0 nM DTX). *$P < 0.05$; **$P < 0.01$; *** $P < 0.001$; (D and E) A combination of DRB18 (10 μM) and increasing DTX concentrations had little to no effect on Ace-1 and PC3 cell viability following 24 h treatment. One-way ANOVA. Different letters indicate statistically significant comparisons ($P < 0.05$); (F) Gene Set Enrichment Analysis (GSEA) performed on metastatic PCa samples from men treated with or without DTX showed statistically significant changes (solid bars) in some metabolic pathways related to fat and carbohydrate metabolism. Metabolic pathways involving glucose import and metabolism were not significantly altered (striped bars) in either combined (orange bars) or bone-only metastases (blue bars). PCa: Prostate cancer (PCa); GLUTs: Glucose transporters.

The effects of DRB18 and DTX on PCa were tested in combination. The two compounds have differing, yet complementary mechanisms of action, as DTX increases reactive oxygen species (ROS) and DRB18 prevents adequate antioxidation[29,55]. However, a combination of the two compounds did not potentiate anti-cancer efficacy. The effects of prolonged DTX therapy on cancer cell metabolism are conflicting[56,57]. However, PC3 cells resistant to DTX upregulated oxidative phosphorylation and decreased GLUT1 expression and glucose uptake *in vitro*[56]. In support of the prolonged effects of DTX on PCa, we found that samples from men with metastatic PCa had no change in gene expression for glucose-related metabolic pathways with DTX therapy. Naïve cells treated with DTX may have an initial increase in glucose import, glycolysis, and ROS, but this did not reflect increased susceptibility to DRB18.

Alteration of glucose homeostasis, leading to a prediabetic state of hyperglycemia and hyperinsulinemia, is a concern with the use of GLUT antagonists. Blood glucose and plasma insulin were measured at the termination of this study. Control and treated mice did not differ, though glucose was trending upward. Previous work suggests hyperglycemia is not a concern with this compound[28]. Triglycerides and free fatty acids are often increased in patients with diabetes mellitus and other causes of hyperglycemia, as lipids and glycerol are consumed as alternative energy sources[58]. Triglycerides primarily enter circulation following dietary absorption or synthesis in the liver[59]. The low plasma triglyceride concentration in this study was likely due to a combination of malnutrition and malassimilation of dietary fats, rather than a direct effect of DRB18.

The results of this study require further consideration. First, only one treatment group was evaluated, and the concentration of DRB18 was altered during the investigation. However, we did not demonstrate anti-tumor efficacy even at the maximum tolerated dose. Second, the small *in vivo* sample size (n = 4-8 per group) could limit statistical power. The results do not suggest that statistical differences between groups were limited by low power. Third, a limitation of biological relevance was the inclusion of only AR negative (AR-) PCa lines. Most PCa cases in men are AR+, including in castration-resistant stages. Studies investigating tumor metabolism in AR+ and AR- PCa variants have been conflicting. GLUT1 was an AR gene target in one study, suggesting that AR+ PCa may favor glycolysis[33]. Tumor hypoxia may additionally promote both GLUT1 and AR expression in PCa[60]. However, research comparing metabolism between AR+ and low/AR- PCa found enhanced glycolysis-related signatures in low/AR- PCa. Importantly, pharmacologically targeting oxidative phosphorylation significantly inhibited the growth of both AR+ and low/AR- PCa in the bone microenvironment of mice[52]. These results suggest glycolysis plays different but relatively unimportant roles in bone metastatic AR+ and AR- PCa.

In conclusion, the inhibition of class I GLUTs with the small molecule DRB18 did not reduce tumor growth in a preclinical model of PCa bone metastasis. Our data underscore that pan-GLUT inhibition may not be effective against advanced PCa and stress the need to test novel compounds under diverse preclinical conditions. The results of this study suggested metastatic PCa, even in the bone environment, grows contrary to Warburg's hypothesis.

DECLARATIONS

Acknowledgments

The authors thank Julie Buckley in the Histology Core Laboratory in the Department of Biomedical Sciences, Ohio University, for assistance in sectioning and staining tissue samples. Graphical abstract was created in part in BioRender. Hoggard, N. (2025) https://BioRender.com/b30p140.

Authors' contributions

Designed overall projects: Hoggard NK, Chen X, Rosol TJ
Performed experiments: Hoggard NK, Szczepaniak MR, Turner MM, LaRussa ZD, Song J, Echols JB
Analyzed and interpreted data: Hoggard NK, Kantake N, Yuan S, Daniels NA, Young JA, Hildreth BE III, Chen X, Rosol TJ
Technical and material support: Kantake N, Yuan S, Bergmeier SC
Manuscript preparation and edit: Hoggard NK, Lo C, Hildreth BE III, Echols JB, Rosol TJ

Availability of data and materials

The material and data that support the findings of this study are available from the corresponding author upon reasonable request.

Financial support and sponsorship

This research was supported by the John J. Kopchick Molecular and Cellular Biology/Translational Biomedical Sciences Research Fellowship Award and the Heritage College of Osteopathic Medicine, Ohio University.

Conflicts of interest

All authors declared that there are no conflicts of interest.

Ethical approval and consent to participate

All experimental mouse procedures were approved by the Ohio University Institutional Laboratory Animal Care and Use Committee (IACUC, protocol number 20-H-019). Male, 5-week-old *NU/J* nude mice were purchased from The Jackson Laboratory (Bar Harbor, ME) and maintained in an AAALAC-accredited facility under conditions of controlled illumination (14:10 h light–dark cycle) and room temperature (22°C). Mice had free access to water and Picolab-irradiated 20% protein rodent diet (Cincinnati Lab Supply, Cincinnati, OH). Upon arrival, mice were quarantined in rodent cages at a density of 4 mice per cage for vivarium acclimation for 4 weeks. Mice were euthanized by combined CO_2 asphyxiation and cervical dislocation in accordance with the AVMA Guidelines for the Euthanasia of Animals.

Consent for publication

Not applicable.

REFERENCES

1. Rawla P. Epidemiology of prostate cancer. *World J Oncol.* 2019;10:63-89. DOI PubMed PMC
2. Siegel RL, Giaquinto AN, Jemal A. Cancer statistics, 2024. *CA Cancer J Clin.* 2024;74:12-49. DOI
3. Bubendorf L, Schöpfer A, Wagner U, et al. Metastatic patterns of prostate cancer: an autopsy study of 1,589 patients. *Hum Pathol.* 2000;31:578-83. DOI
4. Sandhu S, Moore CM, Chiong E, et al. Prostate cancer. *Lancet.* 2021;398:1075-90. DOI
5. Pippione AC, Boschi D, Pors K, Oliaro-bosso S, Lolli ML. Androgen-AR axis in primary and metastatic prostate cancer: chasing steroidogenic enzymes for therapeutic intervention. *J Cancer Metastasis Treat.* 2017;3:328. DOI
6. Blatt EB, Raj GV. Molecular mechanisms of enzalutamide resistance in prostate cancer. *Cancer Drug Resist.* 2019;2:189-97. DOI PubMed PMC
7. Sekino Y, Teishima J. Molecular mechanisms of docetaxel resistance in prostate cancer. *Cancer Drug Resist.* 2020;3:676-85. DOI PubMed PMC
8. Warburg O, Negelein E, Posener K. Versuche an überlebendem carcinomgewebe. *Klin Wochenschr.* 1924;3:1062-4. DOI
9. Warburg O, Wind F, Negelein E. The metabolism of tumors in the body. *J Gen Physiol.* 1927;8:519-30. DOI PubMed PMC
10. Pfeiffer T, Schuster S, Bonhoeffer S. Cooperation and competition in the evolution of ATP-producing pathways. *Science.* 2001;292:504-7. DOI PubMed
11. Pliszka M, Szablewski L. Glucose transporters as a target for anticancer therapy. *Cancers.* 2021;13:4184. DOI PubMed PMC
12. Pragallapati S, Manyam R. Glucose transporter 1 in health and disease. *J Oral Maxillofac Pathol.* 2019;23:443-9. DOI PubMed PMC
13. Younes M, Lechago LV, Somoano JR, Mosharaf M, Lechago J. Wide expression of the human erythrocyte glucose transporter Glut1 in human cancers. *Cancer Res.* 1996;56:1164-7. Available from: https://aacrjournals.org/cancerres/article/56/5/1164/503027/Wide.
14. Szablewski L. Glucose transporters as markers of diagnosis and prognosis in cancer diseases. *Oncol Rev.* 2022;16:561. DOI PubMed PMC
15. Wang T, Wang J, Hu X, Huang XJ, Chen GX. Current understanding of glucose transporter 4 expression and functional mechanisms. *World J Biol Chem.* 2020;11:76-98. DOI PubMed PMC
16. Macheda ML, Rogers S, Best JD. Molecular and cellular regulation of glucose transporter (GLUT) proteins in cancer. *J Cell Physiol.* 2005;202:654-62. DOI
17. Zheng J. Energy metabolism of cancer: glycolysis versus oxidative phosphorylation (Review). *Oncol Lett.* 2012;4:1151-7. DOI PubMed PMC
18. Chen CL, Lin CY, Kung HJ. Targeting mitochondrial OXPHOS and their regulatory signals in prostate cancers. *Int J Mol Sci.* 2021;22:13435. DOI PubMed PMC
19. Butler LM, Centenera MM, Swinnen JV. Androgen control of lipid metabolism in prostate cancer: novel insights and future applications. *Endocr Relat Cancer.* 2016;23:R219-27. DOI PubMed
20. Effert P, Beniers AJ, Tamimi Y, Handt S, Jakse G. Expression of glucose transporter 1 (Glut-1) in cell lines and clinical specimens from human prostate adenocarcinoma. *Anticancer Res.* 2004;24:3057-63. Available from: https://ar.iiarjournals.org/content/24/5A/3057/tab. [Last accessed on 24 Jan 2025]
21. Oyama N, Akino H, Suzuki Y, et al. Prognostic value of 2-deoxy-2-[F-18]fluoro-D-glucose positron emission tomography imaging for patients with prostate cancer. *Mol Imaging Biol.* 2002;4:99-104. DOI
22. Parmar K, Mauch P, Vergilio JA, Sackstein R, Down JD. Distribution of hematopoietic stem cells in the bone marrow according to regional hypoxia. *Proc Natl Acad Sci U S A.* 2007;104:5431-6. DOI PubMed PMC

23. Diedrich JD, Rajagurubandara E, Herroon MK, Mahapatra G, Hüttemann M, Podgorski I. Bone marrow adipocytes promote the Warburg phenotype in metastatic prostate tumors via HIF-1α activation. *Oncotarget.* 2016;7:64854-77. DOI PubMed PMC
24. Spencer JA, Ferraro F, Roussakis E, et al. Direct measurement of local oxygen concentration in the bone marrow of live animals. *Nature.* 2014;508:269-73. DOI PubMed PMC
25. Vaupel P, Höckel M, Mayer A. Detection and characterization of tumor hypoxia using pO_2 histography. *Antioxid Redox Signal.* 2007;9:1221-35. DOI PubMed
26. Zhang Y, Li Q, Huang Z, et al. Targeting glucose metabolism enzymes in cancer treatment: current and emerging strategies. *Cancers.* 2022;14:4568. DOI PubMed PMC
27. Temre MK, Kumar A, Singh SM. An appraisal of the current status of inhibition of glucose transporters as an emerging antineoplastic approach: promising potential of new pan-GLUT inhibitors. *Front Pharmacol.* 2022;13:1035510. DOI PubMed PMC
28. Chen X, Bergmeier SC. Compositions and methods for glucose transport inhibition. US11072576B2, 2021. Available from: https://patents.google.com/patent/US11072576B2/en. [Last accessed on 10 Feb 2025].
29. Shriwas P, Roberts D, Li Y, et al. A small-molecule pan-class I glucose transporter inhibitor reduces cancer cell proliferation in vitro and tumor growth in vivo by targeting glucose-based metabolism. *Cancer Metab.* 2021;9:14. DOI PubMed PMC
30. Liu Y, Zhang W, Cao Y, Liu Y, Bergmeier S, Chen X. Small compound inhibitors of basal glucose transport inhibit cell proliferation and induce apoptosis in cancer cells via glucose-deprivation-like mechanisms. *Cancer Lett.* 2010;298:176-85. DOI
31. Shi Q, Shen Q, Liu Y, et al. Increased glucose metabolism in TAMs fuels O-GlcNAcylation of lysosomal cathepsin B to promote cancer metastasis and chemoresistance. *Cancer Cell.* 2022;40:1207-1222.e10. DOI
32. Jakobsson AW, Kundu S, Guo J, et al. Iron chelator VLX600 inhibits mitochondrial respiration and promotes sensitization of neuroblastoma cells in nutrition-restricted conditions. *Cancers.* 2022;14:3225. DOI PubMed PMC
33. Wang J, Xu W, Wang B, et al. GLUT1 is an AR target contributing to tumor growth and glycolysis in castration-resistant and enzalutamide-resistant prostate cancers. *Cancer Lett.* 2020;485:45-55. DOI
34. LeRoy BE, Thudi NK, Nadella MV, et al. New bone formation and osteolysis by a metastatic, highly invasive canine prostate carcinoma xenograft. *Prostate.* 2006;66:1213-22. DOI
35. Thudi NK, Shu ST, Martin CK, et al. Development of a brain metastatic canine prostate cancer cell line. *Prostate.* 2011;71:1251-63. DOI PubMed PMC
36. Simmons JK, Dirksen WP, Hildreth BE 3rd, et al. Canine prostate cancer cell line (probasco) produces osteoblastic metastases in vivo. *Prostate.* 2014;74:1251-65. DOI PubMed PMC
37. Elshafae SM, Dirksen WP, Alasonyalilar-Demirer A, et al. Canine prostatic cancer cell line (LuMa) with osteoblastic bone metastasis. *Prostate.* 2020;80:698-714. DOI PubMed PMC
38. Simmons JK, Hildreth III BE, Supsavhad W, et al. Animal models of bone metastasis. *Vet Pathol.* 2015;52:827-41. DOI PubMed PMC
39. Chlenski A, Nakashiro K, Ketels KV, Korovaitseva GI, Oyasu R. Androgen receptor expression in androgen-independent prostate cancer cell lines. *Prostate.* 2001;47:66-75. DOI PubMed
40. Yun SJ, Kim SK, Kim J, et al. Transcriptomic features of primary prostate cancer and their prognostic relevance to castration-resistant prostate cancer. *Oncotarget.* 2017;8:114845-55. DOI PubMed PMC
41. Kumar A, Coleman I, Morrissey C, et al. Substantial interindividual and limited intraindividual genomic diversity among tumors from men with metastatic prostate cancer. *Nat Med.* 2016;22:369-78. DOI PubMed PMC
42. Thiemeyer H, Taher L, Schille JT, et al. An RNA-seq-based framework for characterizing canine prostate cancer and prioritizing clinically relevant biomarker candidate genes. *Int J Mol Sci.* 2021;22:11481. DOI PubMed PMC
43. Robinson MD, McCarthy DJ, Smyth GK. edgeR: a Bioconductor package for differential expression analysis of digital gene expression data. *Bioinformatics.* 2010;26:139-40. DOI PubMed PMC
44. Ritchie ME, Phipson B, Wu D, et al. limma powers differential expression analyses for RNA-sequencing and microarray studies. *Nucleic Acids Res.* 2015;43:e47. DOI PubMed PMC
45. Ye J, Coulouris G, Zaretskaya I, Cutcutache I, Rozen S, Madden TL. Primer-BLAST: a tool to design target-specific primers for polymerase chain reaction. *BMC Bioinformatics.* 2012;13:134. DOI PubMed PMC
46. Roberts DA, Wang L, Zhang W, et al. Isosteres of ester derived glucose uptake inhibitors. *Bioorg Med Chem Lett.* 2020;30:127406. DOI
47. Haider M, Zhang X, Coleman I, et al. Epithelial mesenchymal-like transition occurs in a subset of cells in castration resistant prostate cancer bone metastases. *Clin Exp Metastasis.* 2016;33:239-48. DOI PubMed PMC
48. Suwabe Y, Nakano R, Namba S, et al. Involvement of GLUT1 and GLUT3 in the growth of canine melanoma cells. *PLoS One.* 2021;16:e0243859. DOI PubMed PMC
49. Liu Y, Cao Y, Zhang W, et al. A small-molecule inhibitor of glucose transporter 1 downregulates glycolysis, induces cell-cycle arrest, and inhibits cancer cell growth in vitro and in vivo. *Mol Cancer Ther.* 2012;11:1672-82. DOI
50. Chandler JD, Williams ED, Slavin JL, Best JD, Rogers S. Expression and localization of GLUT1 and GLUT12 in prostate carcinoma. *Cancer.* 2003;97:2035-42. DOI PubMed
51. Reinicke K, Sotomayor P, Cisterna P, Delgado C, Nualart F, Godoy A. Cellular distribution of Glut-1 and Glut-5 in benign and malignant human prostate tissue. *J Cell Biochem.* 2012;113:553-62. DOI
52. Mossa F, Robesti D, Sumankalai R, et al. Subtype and site specific-induced metabolic vulnerabilities in prostate cancer. *Mol Cancer*

Res. 2023;21:51-61. DOI

53. Whitburn J, Rao SR, Morris EV, et al. Metabolic profiling of prostate cancer in skeletal microenvironments identifies G6PD as a key mediator of growth and survival. *Sci Adv.* 2022;8:eabf9096. DOI PubMed PMC
54. Jiang H, Liu M, Deng Y, et al. Identification of prostate cancer bone metastasis related genes and potential therapy targets by bioinformatics and in vitro experiments. *J Cell Mol Med.* 2024;28:e18511. DOI
55. Pienta KJ. Preclinical mechanisms of action of docetaxel and docetaxel combinations in prostate cancer. *Semin Oncol.* 2001;28:3-7. DOI PubMed
56. Ippolito L, Marini A, Cavallini L, et al. Metabolic shift toward oxidative phosphorylation in docetaxel resistant prostate cancer cells. *Oncotarget.* 2016;7:61890-904. DOI PubMed PMC
57. Catanzaro D, Gabbia D, Cocetta V, et al. Silybin counteracts doxorubicin resistance by inhibiting GLUT1 expression. *Fitoterapia.* 2018;124:42-8. DOI
58. Ginsberg HN, Zhang YL, Hernandez-Ono A. Regulation of plasma triglycerides in insulin resistance and diabetes. *Arch Med Res.* 2005;36:232-40. DOI PubMed
59. Feingold KR. Lipid and lipoprotein metabolism. *Endocrinol Metab Clin North Am.* 2022;51:437-58. DOI PubMed
60. Cameron S, Deblois G, Hawley JR, et al. Chronic hypoxia favours adoption to a castration-resistant cell state in prostate cancer. *Oncogene.* 2023;42:1693-703. DOI PubMed PMC